Multifunctional Schottky-Diode Circuit Comprising Palladium/Molybdenum Disulfide Nanosheet

*Jin Sung Kim, Hee Sung Lee, Pyo Jin Jeon, Young Tack Lee, Woojin Yoon, Sang-Yong Ju, and Seongil Im**

As one of the promising two dimensional (2D) semiconductors, molybdenum disulfide (MoS_2) nanosheet has recently been attracting much attention from researchers in respects of its relatively high mobility and distinct energy band gap of 1.2–1.8 eV,[1–7] which is different from that of graphene, the gapless 2D semiconductor.[8–12] The magnitude of MoS_2 energy band gap is dependent on the nanosheet thickness;[4–7] single layer sheet appears to have ≈1.8 eV while bulk-type thick layers show 1.2 eV as their band gap. Many applications using MoS_2 nanosheet has thus been reported,[13–20] and those were mostly about top- or bottom-gated field-effect transistors (FETs). However, P-N diode or Schottky diode devices using MoS_2 have hardly been reported yet except few[18–20] while only a couple of P-N diode reports are mostly found with WSe_2 nanosheets,[21,22] although such diode components would be also as important as FETs in circuit. Schottky diode applications are particularly rare in any nanosheets. It is probably because researchers have been mainly interested in the Ohmic-Schottky contact issue of nanosheet FET source-drain,[18,23] rather than in Schottky effect-driven device engineering. Hence, reports on the dynamic rectifications of diode type devices are even less to find yet and any diode circuit integrations for voltage output have not been shown, either.

In the present study, we have fabricated a Palladium (Pd)-driven MoS_2 Schottky diode and its related circuit which has quite a simple form but turns out to be very useful toward multifunctional applications based on the Schottky barrier effects at the Pd/a few layer MoS_2 interface. Our Schottky diode circuits demonstrate desirable static and dynamic behavior as an electrical rectifier, a visible light sensor, and a hydrogen gas sensor with voltage output. Among all the applications our hydrogen gas sensor circuits with 2, 4, and 7 layer (L) MoS_2 appeared as probably the most attractive, to exploit the Schottky barrier between Pd and MoS_2. In particular, Pd/2L-MoS_2 interface turns out to be the most efficient for fast switching dynamics in hydrogen gas sensing due to its largest barrier height among other interfaces with thicker MoS_2.

Figure 1a and its inset respectively display optical microscope (OM) images of 4L thin MoS_2 nanosheet contacted by three- and two-terminal electrodes, where two-terminal electrode is Au/Ti for an Ohmic contact with MoS_2 in the inset and the central one among three terminals in Figure 1a is Pd for Schottky contact. The utilized MoS_2 layers were 2L, 4L, and 7L, while 4L MoS_2 nanosheet was mainly used among them. Figure 1b shows the Raman spectroscopy results from 2L and 4L MoS_2 nanosheets on SiO_2/p^+-Si substrate while 7L MoS_2 thickness was measured by atomic force microscopy (AFM) scan as shown in Supporting Information Figure S1, (where the OM images of 2L, 4L, and 7L are also displayed).[24] When we sweep the device without Pd (Figure 1a inset) with back gate voltage (V_G to p^+-Si), normal transistor transfer curve for drain current–back gate voltage (I_D–V_G) behavior of Figure 1d was obtained, along with corresponding output curves of Figure 1e inset. These indicate that our 4L MoS_2 has been well attached on SiO_2 and Au/Ti contact to MoS_2 is quite Ohmic. However, when the other device with Pd on top (Figure 1a) is swept by back gate V_G, its transfer curve in Figure 1d appears much degraded compared to that of the device without Pd, due to Pd-induced charge depletion in MoS_2 layer. Now the carrier depletion below Pd terminal is schematically displayed in three dimensional view of Figure 1c. The output curves of Figure 1e shows the drain current behavior of Pd-depleted MoS_2 layer. A little asymmetry in the output I-V curves with Pd may occur due to the different Au/Ti-MoS_2 contact area in the two Ohmic terminals.

Based on the device of Figure 1a, two Schottky diodes were formed in the left and right side of the three-terminal electrode as shown in the inset circuit of **Figure 2**b. The two displayed similar typical diode curves (current–voltage (I–V) behavior in linear and logarithmic scales) as shown in Figure 2a. Their ideality factor, η appears to be ≈1.2 and ON/OFF current ratio was more than 100. Recent report mentions Fermi level pinning-induced non-ideality in metal/MoS_2 Schottky contact, which would be related to some of crystalline defects in MoS_2.[25] Nonetheless, all of our diodes with as-patterned Pd/MoS_2 show quite good Schottky behavior with η of 1.2, which indicates that our MoS_2 might have less

J. S. Kim, H. S. Lee, P. J. Jeon, Y. T. Lee, Prof. S. Im
Department of Physics and
Institute of Physics and Applied Physics
Yonsei University
50 Yonsei-ro, Seodaemun-gu, Seoul 120–749, Korea
E-mail: semicon@yonsei.ac.kr
W. Yoon, Prof. S.-Y. Ju
Department of Chemistry
Yonsei University
50 Yonsei-ro, Seodaemun-gu, Seoul 120–749, Korea

DOI: 10.1002/smll.201401046

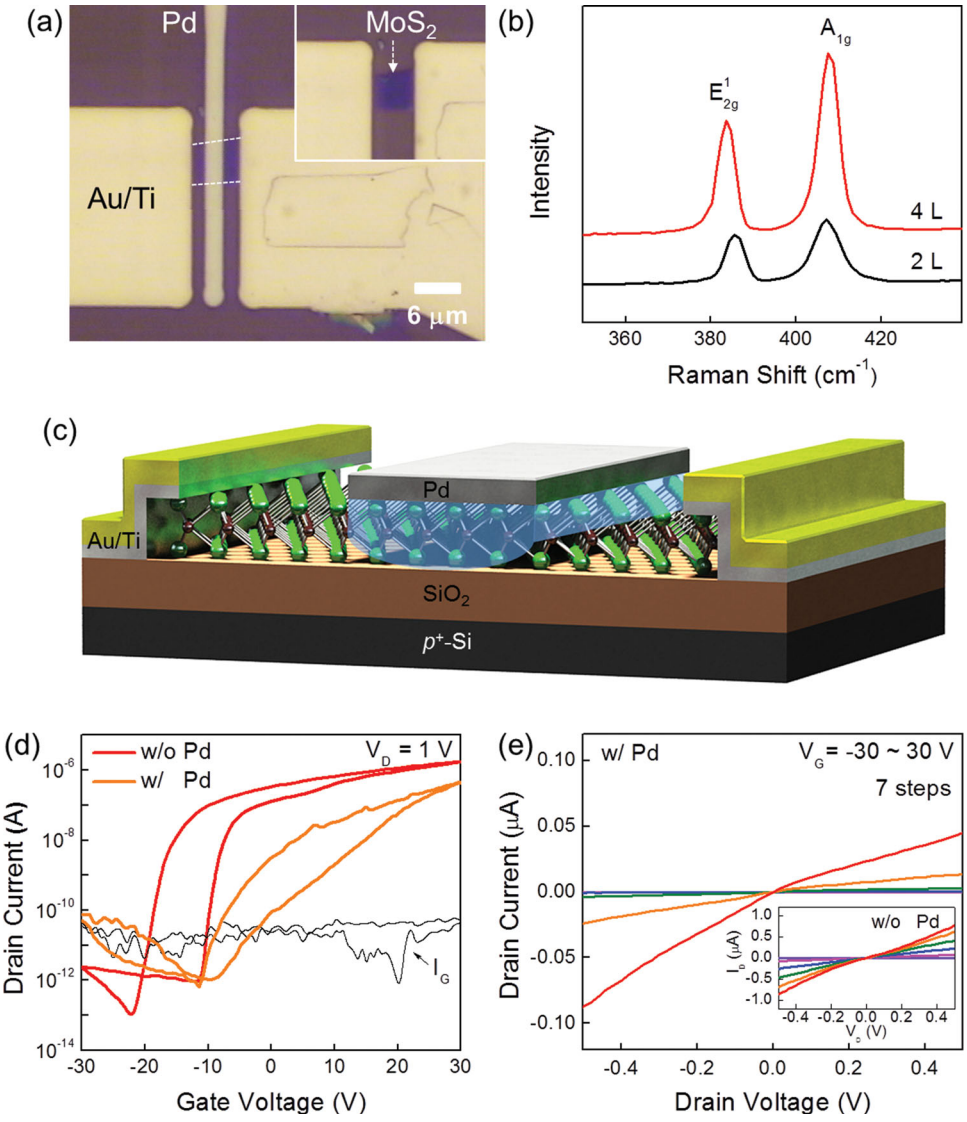

Figure 1. a) Optical microscope images of 4L MoS_2 channel contacted by three- and two-terminal electrodes (inset), where two-terminal electrode is Au/Ti for Ohmic contact and three-terminal device has central Pd electrode for making Schottky contact. b) Raman spectra obtained from 2 and 4L MoS_2 on a 285 nm SiO_2/p^+-Si substrate. c) Three-dimensional schematic view of multifunctional Schottky diode circuit with Pd/hexagonal structured MoS_2 nanosheet (note charge depletion region under Pd). d) Transfer curves of 4L MoS_2 back-gate transistor (with and without Pd Schottky electrode) as obtained at V_D of 1 V. e) I_D–V_D output curves of 4L MoS_2 back-gate transistor measured after (w/) Pd deposition and before (w/o) (inset plot).

density of surface defects. (But post-annealing the Pd/MoS_2 diode at 200 °C degrades the Schottky barrier, probably because Pd contamination to the MoS_2 surface takes place.) Now since the two diodes are connected in series but in opposite back-to-back direction each other, a rectified output voltage (V_{out}) would be measured at the central Pd electrode when one Au/Ti terminal is swept by input voltage (V_{in}) with respect to the other Au/Ti which is grounded. This is a rectifying operation of our back-to-back Schottky diode circuit which has two diodes for one circuit; left diode is forwardly biased when right one is under reverse biases or vice versa during sweep. Such DC voltage sweep then results in a rectified V_{in}–V_{out} curve of Figure 2b according to its inset circuit. Therefore, if we put the device circuit under AC V_{in} bias conditions, we are able to observe dynamic voltage rectification results. Figures 2 and d display such dynamic rectification results with V_{out} as obtained by applying square wave AC V_{in} (–1 to 1 V) at 1 Hz and 5 Hz, respectively. (We attempted 10 Hz operation to measure any V_{out} delay, which was ≈10 ms, as observed from Supporting Information Figure S2. So, maximum 100 Hz operation can be promised to be a upper bound of our recification dynamics.) Similar circuits were also implemented with Ni/ZnO nanowire Schottky diodes at a little higher frequencies as reported in the literature.[26]

Figure 3a shows the photocurrent signals obtained from our diodes with 4L MoS_2 under light emitting diodes for red (R: 630 nm), green (G: 550 nm), blue (B: 440 nm) photons (see the inset for the measurement configuration). Photocurrent appears more sensitively gained under reverse bias conditions than forward biases.[27] It is because the Schottky barrier-induced depletion zone would be extended to lateral side of nanosheet from the thickness region beneath

small 2014,
DOI: 10.1002/smll.201401046

NANO MICRO small

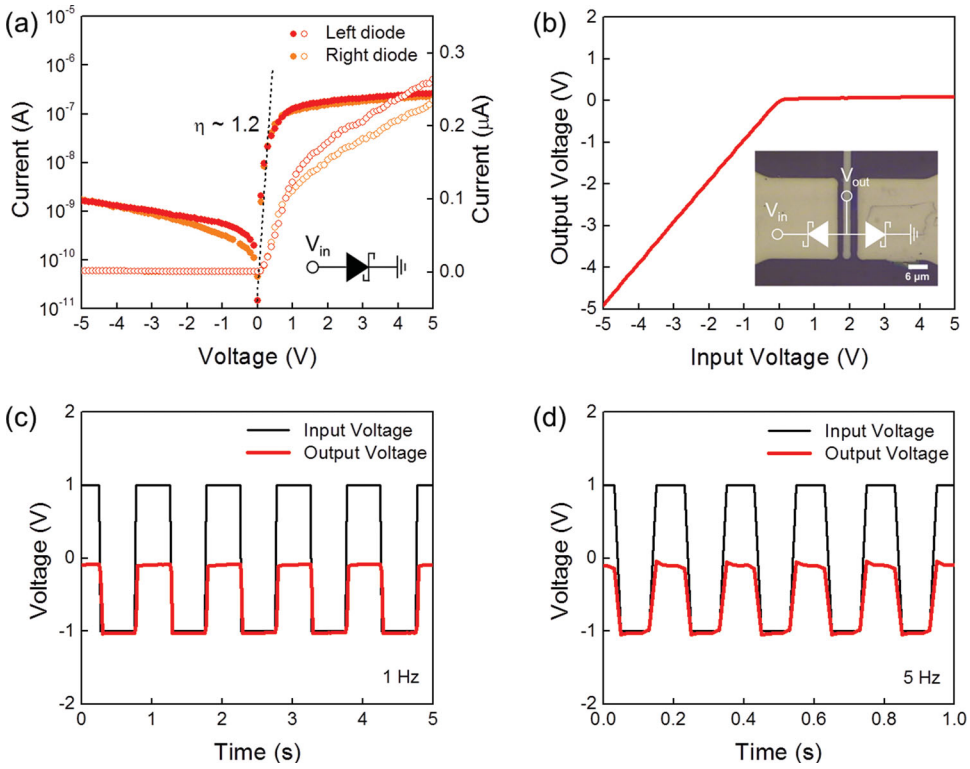

Figure 2. a) Current–voltage curves obtained from the left and right side MoS_2/Pd Schottky diodes. b) V_{in}–V_{out} curve of our back-to-back Schottky diode circuit with sweeping input voltage in a range of $V_{in} = -5$ V to 5 V. The inset photo shows an optical microscope image of our device along with circuit configuration. Rectified dynamic voltage output was also obtained by applying AC square wave input at c) 1 Hz and d) 5 Hz.

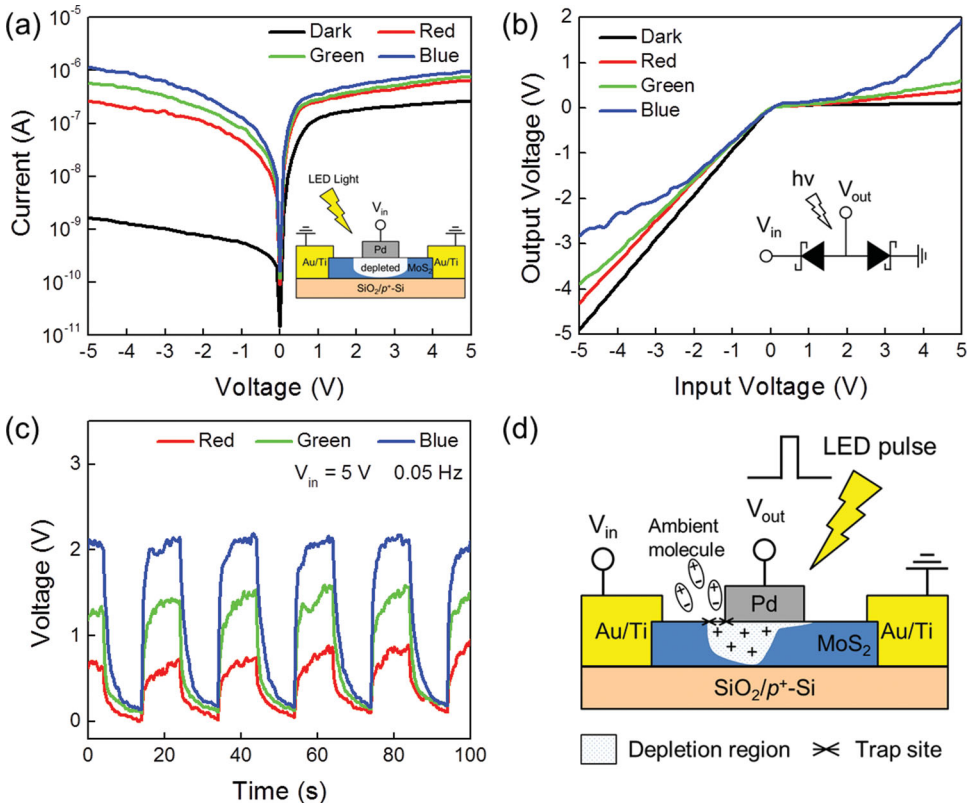

Figure 3. Photo-induced a) *I*–*V* curves of Schottky diode (inset) and b) V_{in}–V_{out} curves of back-to-back circuit device as obtained under red, green, and blue LED illuminations. c) Photo-induced voltage dynamics with 0.05 Hz pulsed (20 s period) LED lights. d) Cross sectional schematic of our device, whose channel is asymmetrically depleted and under pulsed light. Ambient molecules with dipole moment can be adsorbed on the depleted surface.

DOI: 10.1002/smll.201401046

Pd by applying reverse biases,[28,29] so that the photo-excited charges may effectively be harvested through those extended depletion regions as indicated by the inset scheme. This Schottky-driven photodiode is now transformed to a photo-sensing device which is able to extract photo-induced V_{out} signal by properly determined DC voltage V_{in} (as seen in the inset circuit scheme of Figure 3b). Figure 3b displays photo-induced and dark V_{in}–V_{out} curves obtained by DC V_{in} sweep under R, G, and B LED illuminations, which have a similar optical power of ≈2 mW. Dark V_{in}–V_{out} curve was flat (V_{out} = 0) in positive V_{in} region which indicates reverse-bias for the left diode as in the case of Figure 2b. When the visible LED lights illuminate the device circuit (inset), positive V_{out} values are obtained. As in the case of photocurrent generation (Figure 3a), higher energy photons such as blue always brought higher spectral sensitivity in photo-induced V_{out}. This spectral sensitivity difference is comparable and similar to our previous results from phototransistors with 3L MoS_2.[5] As a next step of photo-sensing experiment on the device, we implemented a photo-dynamic property characterization to examine the photo-switching speed of our device, which can be performed at a fixed V_{in} of 5 V by turning on and off the light in 20 s period. As a result, the photo-dynamics of V_{out} has been achieved in time domain as shown in Figure 3c, according to which off-dynamics appears as slow as longer than 5 s for decay time. The long decay is probably due to trap-induced dark current originating from photo-carriers trapped at the surface of laterally-depleted zone.[30] Figure 3d shows the schematic cross section of our photo-sensing device under a V_{in} of 5 V and on/off LED pulse. Since left side Schottky diode is reverse-biased while right side one is forward-biased, the depletion region should be asymmetric and deviated from the beneath of central Pd location. Before light illumination, the depleted surface of the thin MoS_2 would be electrically positive attracting some dipole moment-containing molecules (adsorption).[31–33] During the light introduction to the region, some of photo-generated electrons release those surface molecules (desorption) and are trapped at the surface while others move to V_{in} terminal. (Photo-generated holes are drained to the ground). Soon after the light off, the surface is again depleted with (+) polarity to adsorb the ambient molecules, and the depletion state with (+) polarity simultaneously retards the remaining surface-trapped electrons that want to move toward V_{in} terminal, operating as the source of persistent photoconductivity (PPC). In general, photo-sensitivity in MoS_2 would be most effectively acquired by back-gated FET devices,[30] but our Schottky device is also regarded as a practical photo-sensing device although its sensitivity is less than that of FETs.

As a last experiment for a sensor device, we implemented hydrogen gas (H_2) sensing using the same Pd/MoS_2 Schottky diode circuit but with three different thickness layers of MoS_2: 2L, 4L, and 7L. This measurement is based on two important facts reported in literature; firstly, hydrogen gas makes the work function of Pd small causing phase transformation from Pd to PdH_x,[34–36] which is reversible, and next is that a thinner MoS_2 has a larger band gap. According to *I*–*V* curves of **Figure 4**a obtained from the Schottky diodes

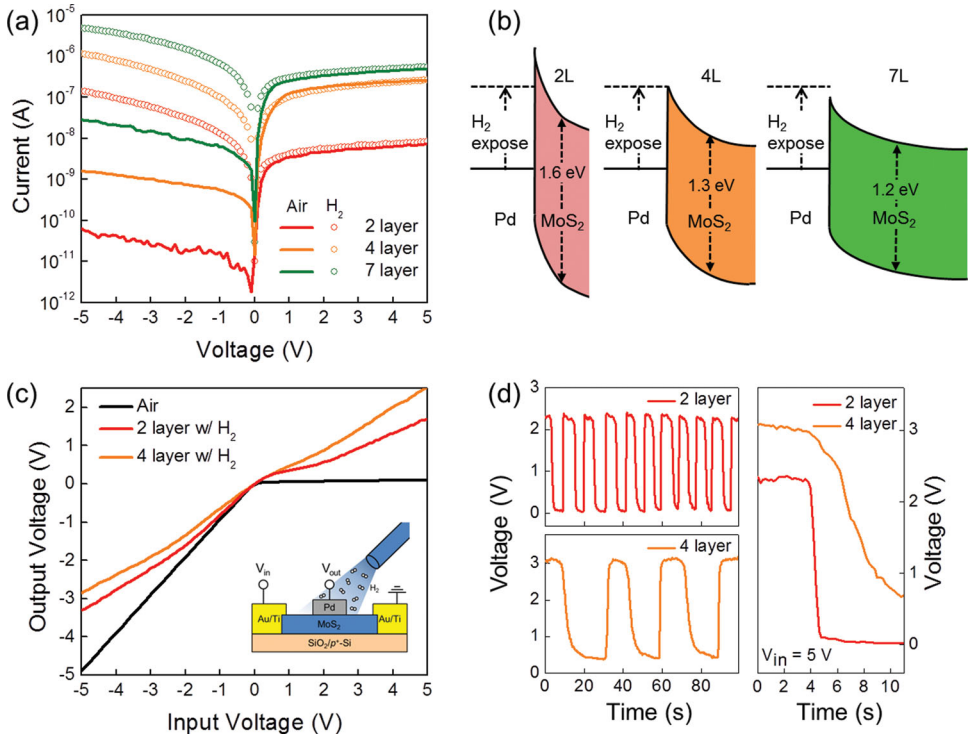

Figure 4. a) Current–voltage curves obtained from 2, 4, and 7L MoS_2 diodes without and with hydrogen gas. b) Thickness-dependent band diagrams of MoS_2 with Pd contact, Pd-induced Schottky barrier height. After H_2 exposure, the barrier height decreases to an overcoming point for electron transfer. c) V_{in}–V_{out} curves of 2L and 4L back-to-back circuit devices with and without H_2 gas. Inset scheme shows H_2 sensing experiments. d) Time domain voltage responses as obtained from our devices with repeated H_2 exposure. Right side plot shows a magnified recovery delay of 2L and 4L MoS_2 devices.

small 2014,
DOI: 10.1002/smll.201401046

with (empty circle symbols) and without hydrogen gas (solid lines), those two facts are clearly reflected. Infused by 1% H_2 gas (see the inset of Figure 4c), all the Schottky diodes react with the gas providing so significant amount of leakage current under reverse biases that the reverse current is even higher than forward current. In particular, the reverse bias-induced current of 2L diode is initially the smallest to be less than ≈100 pA at –5 V but shoots up to more than 0.1 μA by 1% H_2 gas infusion, which is three orders of magnitude higher than initial value (without H_2). This signifies that under the hydrogen gas ambient the work function level of Pd becomes small enough to overcome the Schottky barrier or overcome the conduction band edge of MoS_2.[36–41] According to the literature,[35,36,39,40] Pd work function level may rise up by more than 1.2 eV (from 5.2 to ≈4 eV) according to H_2 gas adsorption that often leads to Pd-to-PdH_x phase transformation. In more details of Figure 4a, we could also see that without H_2 ambient the reverse bias-induced current (solid lines) in 2L diode is much smaller than those of 4L and 7L diodes. It is because the 2L MoS_2 with larger band gap forms higher Schottky barrier to Pd than those by other thicker MoS_2 as illustrated in the schematic band diagrams of Figure 4b. In this regard, it is understandable that the Schottky diode with 7L MoS_2 shows a largest dark leakage current among the three diode curves at a reverse bias.

With a similar manner implemented for photo-detecting circuits in Figures 3 and c, H_2 gas and its pulses were applied to our back-to-back Schottky diode[42,43] circuit which is shown in the inset of Figure 4c. H_2-induced V_{out} was recorded by Pd electrode for 2L and 4L MoS_2 nanosheets as plotted in V_{in}–V_{out} curves of Figure 4c when V_{in} sweep was implemented with one Au/Ti terminal (while the other terminal was ground). For instance at 5 V of V_{in}, V_{out} is initially zero since left side Schottky diode is reverse-biased and right side one is forward-biased. According to the *I–V* curves of Figure 4a, the diodes under forward bias condition show little reaction/detection with H_2, so H_2-induced V_{out} or gas-induced rectification is simply expected by left side Schottky diode, displaying 2–3 V output signal at 5 V input in Figure 4c. Interestingly, there was no H_2 detection by MoS_2 surface itself as far as we carried out separate experimentations with bare surface MoS_2 flake (see Supporting Information Figure S3), so our detection measurements are only dependent on the variation of Pd work function and Pd/MoS_2 Schottky barrier. When the H_2 gas detection was dynamically implemented, time domain V_{out} behavior of Figure 4d was achieved from 2L and 4L diodes by pulsing 1% H_2 gas onto our devices. According to the time domain curves, switching on-reaction is faster than switching off-reaction, since Pd-to-PdH_x transformation is known to be faster than the reverse way of transformation in general.[44] More interestingly, the 2L MoS_2 Schottky diode circuit apparently displays faster switching off-reaction (≈500 ms) than 4L MoS_2 circuit (more than 5 s) when the H_2 infusion was cut off. The similar slow off-reaction was also shown from 7L MoS_2 circuit (see Supporting Information Figure S4). This switch-off dynamics would be directly related to the individual Schottky barrier heights of the respective MoS_2 layers. When PdH_x is reversibly transformed to Pd with H_2 depletion, Pd/MoS_2 Schottky interface system recovers its barrier height. In this moment, the electrical resistance of 2L base Schottky diode should be more rapidly increased than other diodes with thicker MoS_2 under a same reverse bias because its own barrier height was initially larger than those of the others. Now even small change of work function during PdH_x-to-Pd transformation gains large resistance in 2L case, forming a clear Schottky barrier; 4L and thicker MoS_2 layers may not meet the barrier yet at the same time. In view of the H_2 detection results, it is regarded that the hydrogen sensor application with 2, 4, and 7 L MoS_2 is one of the most attractive among many to exploit the Schottky barrier between Pd and MoS_2.

In summary, we have fabricated a Pd-driven MoS_2 Schottky diode and its related circuit which has quite a simple form comprised of two diodes (connected in series with back-to-back form) but turns out to be useful toward multifunctional applications based on the Schottky barrier effects at the Pd/ a few layer MoS_2 interface. Our Schottky diode circuits demonstrate desirable static and dynamic behavior as an electrical rectifier, a visible light sensor, and a hydrogen gas sensor with voltage output. In particular, our hydrogen gas sensor circuits with 2, 4, and 7L MoS_2 the most effectively display the benefits from Schottky barrier between Pd and MoS_2, also demonstrating that Pd/2L MoS_2 interface is the most efficient for fast switching dynamics due to its larger barrier height than those of other interfaces with thicker MoS_2. We conclude that our Pd/MoS_2 Schottky diode circuit is quite promising and effective due to its simplicity in design and fabrication but also due to its multi-functionality in application.

Experimental Section

Exfoliation and Characterization of MoS_2: Both single-layer and few-layer MoS_2 nanosheets were formed with a mechanical exfoliation method using scotch tape from single crystal bulk MoS_2 (SPI supplies, natural molybdenite) on 285 nm SiO_2 on p^+-doped silicon substrate. Our MoS_2 nanosheet flakes were as large as ≈10 μm in one side, so that a long 6 μm channel was possible in our device (W/L ratio was ≈5.5/6 μm). It has previously found that the layer number of MoS_2 nanosheet can be conjectured by optical microscope observation but is clearly identified by Raman spectroscopy.

MoS_2-based Schottky Diode and Back-to-Back Diode Circuit Fabrication: Both We patterned source (S) and drain (D) electrodes using photo-lithography and lift-off processes. First, the spin coating process was performed to form the lift-off layer (LOR 3A, Micro Chemical) and photo-resist (AZ GXR-601, AZ electronic materials) layers. Then the substrate was exposed to ultraviolet (UV) light with photo-mask for our S/D electrode pattern. After developing patterns, 25/50 nm-thick Au/Ti bilayer for S/D contact was deposited by DC magnetron sputtering system. The lift-off process was done using acetone and LOR remover. After S/D electrodes patterning, MoS_2 sample was annealed using Rapid Thermal Annealing (MILA-3000, SINKU-RIKO) in N_2 gas (99.999% purity) ambient at 300 °C for 10 min to improve Ohmic contact (or to remove any residual photo-resist). Then, for the Schottky contact and hydrogen sensing, 50 nm-thick Pd electrode was patterned and deposited by the same photo-lithography and DC sputtering system.

Electrical, Photo-detecting, and Hydrogen-sensing Characterizations: All the static electrical measurements of our devices were

DOI: 10.1002/smll.201401046

performed with a semiconductor parameter analyzer (HP 4155C, Agilent Technologies) in the dark box at room temperature. Electrical dynamic rectifying characteristics of our MoS_2 Schottky diode and its circuit under various alternating current (AC) conditions were measured by using a function generator (AFG 3022B, Tektronix) and an oscilloscope (TDS 2014B, Tektronix). Photodetecting actions were measured with three different wavelength (red λ = 620 nm, green 520 nm, and blue 470 nm) using LEDs. The optical power of the LEDs was given as ≈2 mW for red, green, and blue in the same distance from the target device. Hydrogen sensing measurements were carried out in the dark box at room temperature with gas-ejecting tube which was connected to a gas bomber of 99% N_2 and 1% H_2 mixture. The gas flowing rate of 1000 sccm was delicately controlled by a regulator for H_2 input whereas no intentional gas was used to purge remnant H_2 gas in the Pd sensing metal.

Supporting Information

Supporting Information is available from the Wiley Online Library or from the author.

Acknowledgements

The authors acknowledge the financial support from NRF (NRL program: Grant No. 2014R1A2A1A01004815), Nano-Materials Technology Development Program (Grant No. 2012M3A7B4034985) and Brain Korea 21 plus Program. "Jin Sung Kim and Hee Sung Lee contributed equally to this work."

[1] J. N. Coleman, M. Lotya, A. O'Neill, S. D. Bergin, S. D. Bergin, P. J. King, U. Khan, K. Young, A. Gaucher, S. De, R. J. Smith, I. V. Shvets, S. K. Arora, G. Stanton, H.-Y. Kim, K. Lee, G. T. Kim, G. S. Duesberg, T. Hallam, J. J. Boland, J. J. Wang, J. F. Donegan, J. C. Grunlan, G. Moriaty, A. Shmeliov, R. J. Nicholls, J. M. Perkins, E. M. Grieveson, K. Theuwissen, D. W. McComb, P. D. Nellist, V. Nicolosi, *Science* **2011**, *331*, 568–571.
[2] B. Radisavlhevic, A. Radenovic, J. Brivio, V. Giacometti, A. Kis, *Nat. Nanotechnol.* **2011**, *6*, 147–150.
[3] C. L. Stender, E. C. Greyson, Y. Babayan, T. W. Odom, *Adv. Mater.* **2005**, *17*, 2837–3841.
[4] M. Chhowalla, H. S. Shin, G. Eda, L.-J. Li, K. P. Loh, H. Zhang, *Nat. Chem.* **2013**, *5*, 263–275.
[5] H. S. Lee, S.-W. Min, Y.-G. Chang, M. K. Park, T. Nam, H. Kim, J. H. Kim, S. Ryu, S. Im, *Nano Lett.* **2012**, *12*, 3695–3700.
[6] K. F. Mak, C. Lee, J. Hone, J. Shan, T. F. Heinz, *Phys. Rev. Lett.* **2010**, *105*, 136805.
[7] Q. H. Wang, K. Kalantar-Zadeh, A. Kis, J. N. Coleman, M. S. Strano, *Nat. Nanotechnol.* **2012**, *7*, 699–712.
[8] A. K. Geim, *Science* **2009**, *324*, 1530–1534.
[9] K. S. Novoselov, D. Jiang, F. Schedin, T. J. Booth, V. V. Khotkevich, S. V. Morozov, A. K. Geim, *Proc. Natl. Acad. Sci. U.S.A.* **2005**, *102*, 10451–10453.
[10] K. S. Novoselov, A. K. Geim, S. V. Morozov, D. Jiang, Y. Zhang, S. V. Dubonos, I. V. Grigorieva, A. A. Firsov, *Science* **2004**, *306*, 666–669.
[11] M. Y. Han, B. Özyilmaz, Y. Zhang, P. Kim, *Phys. Rev. Lett.* **2007**, *98*, 206805.
[12] B. K. Bolotin, K. J. Sikes, Z. Jiang, M. Klima, G. Fudenberg, J. Hone, P. Kim, H. L. Stormer, *Solid State Commun.* **2008**, *146*, 351–355.
[13] H. S. Lee, S.-W. Min, M. K. Park, Y. T. Lee, P. J. Jeon, J. H. Kim, S. Ryu, S. Im, *Small* **2012**, *8*, 3111–3115.
[14] H. Li, Z. Yin, Q. He, H. Li, X. Huang, G. Lu, D. W. H. Fam, A. I. Y. Tok, Q. Zhang, H. Zhang, *Small* **2012**, *8*, 63–67.
[15] H. Wang, L. Yu, Y.-H. Lee, Y. Shi, A. Hsu, M. L. Chin, L.-J. Li, M. Dubey, J. Kong, T. Palacios, *Nano Lett.* **2012**, *12*, 4674–4680.
[16] Z. Yin, H. Li, H. Li, L. Jiang, Y. Shi, Y. Sun, G. Lu, Q. Zhang, X. Chen, H. Zhang, *ACS Nano* **2012**, *6*, 74–80.
[17] B. Radisavljevic, M. B. Whitwick, A. Kis, *ACS Nano* **2011**, *5*, 9934–9938.
[18] J.-R. Chen, P. M. Odenthal, A. S. Swartz, G. C. Floyd, H. Wen, K. Y. Luo, R. K. Kawakami, *Nano Lett.* **2013**, *13*, 3106–3110.
[19] M. Fontana, T. Deppe, A. K. Boyd, M. Rinzan, A. Y. Liu, M. Paranjape, P. Barbara, *Sci. Rep.* **2013**, *3*, 1634.
[20] D. Jariwala, V. K. Sangwan, C.-C. Wu, P. L. Prabhumirashi, M. L. Geier, T. J. Marks, L. J. Lauhon, M. C. Hersam, *Proc. Natl. Acad. Sci. U.S.A.* **2013**, *110*, 18076–18080.
[21] S. Chuang, R. Kapadia, H. Fang, T. C. Chang, W.-C. Yen, Y.-L. Chueh, A. Javey, *Appl. Phys. Lett.* **2013**, *102*, 242101.
[22] B. W. H. Baugher, H. O. H. Churchill, Y. Yang, P. Jarillo-Herrero, *Nat. Nanotechnol.* **2014**, *9*, 262–267.
[23] S. Das, H.-Y. Chen, A. V. Penumatcha, J. Appenzeller, *Nano Lett.* **2013**, *13*, 100–105.
[24] C. Lee, H. Yan, L. E. Brus, T. F. Heinz, J. Hone, S. Ryu, *ACS Nano* **2010**, *4*, 2695–2700.
[25] S. McDonnell, R. Addou, C. Buie, R. M. Wallace, C. L. Hinkle, *ACS Nano* **2014**, *3*, 2880–2888.
[26] B. Ryu, Y. T. Lee, K. H. Lee, R. Ha, J. H. Park, H.-J. Choi, S. Im, *Nano Lett.* **2011**, *11*, 4246–4250.
[27] R. S. Muller, T. I. Kamins, M. Chan, *Device Electronics for Integrated Circuits*, Johns Wiley & Sons, New York, USA **2003**.
[28] F. Léonard, A. A. Talin, *Nat. Nanotechnol.* **2011**, *6*, 773–783.
[29] F. Léonard, J. Tersoff, *Phys. Rev. Lett.* **1999**, *83*, 5174–5177.
[30] O. Lopez-Sanchez, D. Lembke, M. Kayci, A. Radenovic, A. Kis, *Nat. Nanotechnol.* **2013**, *8*, 497–501.
[31] K. Cho, W. Park, J. Park, H. Jeong, J. Jang, T.-Y. Kim, W.-K. Hong, S. Hong, T. Lee, *ACS Nano* **2013**, *7*, 7751–7758.
[32] K. Cho, T.-Y. Kim, W. Park, J. Park, D. Kim, J. Jang, H. Jeong, S. Hong, T. Lee, *Nanotechnology* **2014**, *25*, 155201.
[33] W. Zhang, J.-K. Huang, C.-H. Chen, Y.-H. Chang, Y.-J. Cheng, L.-J. Li, *Adv. Mater.* **2013**, *25*, 3456–3461.
[34] Y. T. Lee, H. Jung, S. H. Nam, P. J. Jeon, J. S. Kim, B. Jang, W. Lee, S. Im, *Nanoscale* **2013**, *5*, 8915–8920.
[35] Y. Sun, H. H. Wang, *Adv. Mater.* **2007**, *19*, 2818–2823.
[36] R. Du , E. Nowicka, Z. Wolfram, *Surf. Sci.* **1989**, *216*, 1–13.
[37] S. N. Das, A. K. Pal, *J. Phys. D: Appl. Phys.* **2007**, *40*, 7291–7297.
[38] J. Kim, F. Ren, B. P. Gila, C. R. Abernathy, S. J. Pearton, *Appl. Phys. Lett.* **2003**, *82*, 739–741.
[39] N. Yamamoto, S. Tonomura, T. Matsuoka, H. Tsubomura, *Surf. Sci.* **1980**, *92*, 400–406.
[40] R. Du , R. Nowakowski, E. Nowicka, *J. Alloys Compd.* **2004**, *404–406*, 284–287.
[41] K. ITO, *Surf. Sci.* **1979**, *86*, 345–352.
[42] A. J. Chiquito, C. A. Amorim, O. M. Berengue, L. S. Araujo, E. P. Bernardo, E. R. Leite, *J. Phys.: Condensed Matter* **2012**, *24*, 225303.
[43] M. B. Reine, P. W. Norton, R. Starr, M. H. Weiler, M. Kestigian, B. L. Musicant, *J. Electron. Mater.* **1995**, *24*, 669–679.
[44] E. Lee, J. M. Lee, J. H. Koo, W. Lee, T. Lee, *Inter. J of Hydro. Ener.* **2010**, *35*, 6984–6991.

Received: April 15, 2014
Revised: June 20, 2014
Published online:

DOI: 10.1002/smll.201401046